Recombination of Br− 2 photodissociated within mass selected ionic clusters

Michael L. Alexander, Nancy E. Levinger, M. A. Johnson, Douglas Ray, and W. C. Lineberger

Citation: The Journal of Chemical Physics **88**, 6200 (1988); doi: 10.1063/1.454458
View online: http://dx.doi.org/10.1063/1.454458
View Table of Contents: http://scitation.aip.org/content/aip/journal/jcp/88/10?ver=pdfcov
Published by the AIP Publishing

Recombination of Br_2^- photodissociated within mass selected ionic clusters

Michael L. Alexander, Nancy E. Levinger, M. A. Johnson,[a] Douglas Ray, and W. C. Lineberger

Department of Chemistry, University of Colorado and Joint Institute for Laboratory Astrophysics, University of Colorado and National Bureau of Standards, Boulder, Colorado 80309

(Received 19 November 1987; accepted 3 February 1988)

Photofragmentation studies of mass selected $Br_2^- \cdot (CO_2)_n$, $n \leqslant 24$, cluster ions are presented. The heterogeneous cluster ions are synthesized in a supersonic expansion crossed with an electron beam. These ionic clusters are mass analyzed in a time-of-flight mass spectrometer prior to photodissociation of the Br_2^- absorber in the cluster. Mass analysis of the ionic photofragments shows that in some cases the photodissociated Br_2^- has recombined and in other cases a Br atom has escaped from the cluster. The branching ratio for recombination depends on both the size of the initial cluster ion and the photodissociation wavelength. The photofragmentation data are consistent with a recombination mechanism dominated by attractive forces in the smaller clusters and repulsive interactions in the larger clusters.

I. INTRODUCTION

Among the more promising prospects for cluster research is the possibility of using appropriate molecular clusters to model the microscopic behavior of certain chemical and physical processes normally masked by the inherent averaging of observations on bulk samples.[1] For example, clusters have been used as a means of localizing reactants in a chemical reaction[2] and as a means of preparing them in well defined orientations.[3] Clusters can also be used to explore the effects of solvation on the energetics and dynamics of chemical reactions. This paper concerns the photodissociation and recombination of a diatomic molecule interacting with a specific number of solvent molecules in a molecular cluster.

Photodissociation and recombination of the dihalogens, particularly I_2, have been studied extensively. Noyes and coworkers measured the photolysis quantum yield as a function of excitation wavelength[4] and viscosity[5] in a variety of solvents and emphasized the need for a molecular level description of the reaction.[6] More recently, measurement of the photolysis quantum yields and the atom–atom recombination rates of I_2, Br_2, and Cl_2 have been performed in both the gas phase[7–12] and the liquid phase[13,14] at a variety of pressures and temperatures[15] using laser-based techniques. Troe and co-workers have suggested that van der Waals clusters are important in decreasing the photolysis quantum yield under certain conditions.[12,14] Picosecond pump–probe experiments have been performed on I_2 in solution to determine the time scales of atom–atom geminate recombination and vibrational relaxation of the recombined diatom by solvent molecules.[16] The process has also been investigated theoretically by numerous investigators in order to understand the observed behavior.[16] Photodissociation and recombination of the dihalogens have also been investigated in rare gas matrices[17,18] where the state distribution of the nascent I_2^* or Br_2^* was determined by time resolving the dispersed fluorescence from species recombining on excited state potential energy surfaces. These studies indicated that the relaxation pathway was strongly dependent on the solvent cage.[18]

Photodissociation and recombination in clusters have been studied by only a few investigators. In laser induced fluorescence measurements on $I_2 \cdot Ar_n$ clusters synthesized in a free jet expansion,[19,20] I_2 fluorescence was detected even when I_2 was excited above its dissociation limit. Valentini and Cross[20] have observed fluorescence from I_2 following excitation of $I_2 \cdot Ar$ above the dissociation limit of I_2, leading to the suggestion that one atom is sufficient to cage the nascent iodine atoms. The photodissociation and subsequent dynamics of Br_2 in $Br_2 \cdot Ar_n$ clusters have been modeled by Amar and Berne.[21] Amar has also modeled[22] the dynamics of $Br_2^- \cdot Ar_n$ clusters following photodissociation of Br_2^-. Both molecular dynamics simulations show a correlation between structure and recombination mechanism; argon atoms approximately collinear with Br_2 or Br_2^- are especially effective at facilitating recombination.

The studies discussed above raise interesting questions concerning photodissociation and recombination within clusters, notably:

(I) How many solvent molecules are necessary to effect recombination?

(II) What is the excitation energy dependence of the propensity of a given cluster to cage the dissociated diatom?

To study these questions, it is essential to synthesize and isolate clusters of specific composition, photodissociate the diatom within the cluster and then detect the photoproducts. Ionic clusters are ideally suited for these experiments since the isolation can be achieved by mass analysis. A number of groups have reported instruments which provide this capability.[23–30] Except for recent work by Bowers and coworkers on photoinduced charge transfer,[23] these groups have not explored photoinduced chemistry.

In this work we investigate the photodissociation of Br_2^- ions solvated by a specific number of CO_2 molecules and probe the dynamics of the ensuing Br–Br^- recombination. The experiments are performed with a tandem time-of-flight

[a] Present address: Department of Chemistry, Yale University, New Haven, Connecticut.

 0021-9606/88/106200-11$02.10

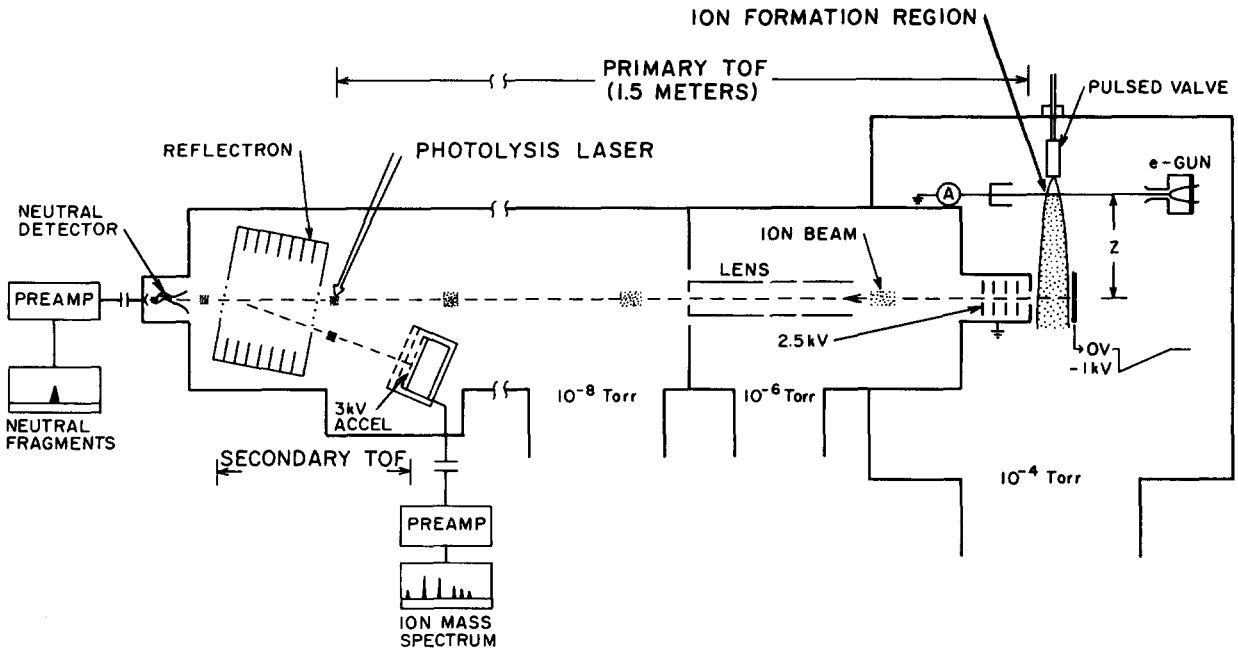

FIG. 1. A schematic diagram of the experimental apparatus showing the three main regions: ion formation, primary TOF, and secondary TOF. In the first region, ions are formed by the interaction of an electron beam with a pulsed free jet expansion. The ions drift downstream, react with the neutral gas forming cluster ions and are extracted into the primary TOF. In the primary TOF, the cluster ions are separated in time according to their mass where the pulsed laser beam crosses the cluster ion beam. In the secondary TOF, ionic photofragments and parent ions are separated in time according to their mass by a reflectron. The ions are detected by a particle multiplier. Neutral photofragments pass through the reflectron where they are detected by a separate particle multiplier.

(TOF) mass spectrometer, the first stage is used to select a particular cluster ion for laser interaction and the second stage is employed to determine the composition of the ionic photofragments. We report the branching ratio for recombination of the photoinduced Br and Br^- atoms to form Br_2^- as a function of the photodissociation wavelength and the number of CO_2 solvent molecules. Three distinct regions of photofragmentation behavior are observed as a function of cluster size. The data are interpreted in terms of Amar's recent theoretical work on $Br_2^- \cdot Ar_n$ clusters.[22] His studies indicate that for smaller clusters, recombination occurs due to the attractive forces between the diatom and the solvent molecules while, for larger clusters, recombination is effected by impulsive collisions with the solvent molecules.

II. EXPERIMENTAL

A. Overview

A schematic diagram of the apparatus is shown in Fig. 1. It is similar to the apparatus used in our earlier work on $(CO_2)_n^-$ and $(CO_2)_n^+$ cluster ions.[33–35] The $Br_2^- \cdot (CO_2)_n$ cluster ions are created by crossing a pulsed free jet expansion with a continuous 1 keV beam of electrons. Expansion conditions are chosen such that neutral clustering is not extensive. Br_2^- is the primary anion formed following electron beam excitation. $Br_2^- \cdot (CO_2)_n$ clusters grow by ion–molecule association reactions while drifting with the unskimmed expansion. Ions are separated from the free jet by a transverse high voltage pulse which extracts them through an aperture into the first stage of TOF mass analysis. They are then further accelerated to a total beam energy of 3 keV. This two field mass spectrometer separates ions in time, according to their mass, 1.5 m from the aperture. The pulsed laser beam crosses the ion beam at this location. Ionic photofragments and parent ions are mass analyzed by a second, reflectron, TOF mass spectrometer and detected by a particle multiplier after an additional flight segment. Timing of the apparatus is controlled by a computer in conjunction with various delay circuits. Mass spectra of parent and photofragment ions are acquired with a transient digitizer/signal averager. The apparatus can readily be adjusted for positive or negative ion studies; the specific conditions discussed here are for negatively charged clusters.

B. Ion formation

A pulsed free jet expansion provides relatively high neutral molecule densities which, when combined with high energy (1 keV) electron beam excitation, yields a simple and effective method for the preparation of both positively and negatively charged clusters. The pulsed expansion is generated by a solenoid-actuated valve (General Valve series 9) with a 400 μm diam aperture. It delivers gas pulses of 500 μs duration at a repetition rate of 10 Hz. The repetition rate is determined by the use of a pulsed laser with a 10 Hz repetition rate. The backing pressure varies from 1 to 5 atm depending on the system under study. The expansion region is pumped by a 10 in. diffusion pump which maintains a pressure of $1–5 \times 10^{-4}$ Torr under these conditions. For the typical expansion conditions, neutral clustering is not extensive. The positive ions produced directly by the electron beam are primarily monomers and small clusters. The negative ions

produced by low energy electron attachment to neutral species in the jet are also primarily monomers and small clusters.

The electron beam source is a modified cathode ray tube electron beam source. It consists of a filament, followed by acceleration plates, a three element einzel lens, and horizontal and vertical deflectors. The original oxide cathode was easily poisoned; it has been replaced by a thoriated iridium filament. This arrangement produces a well collimated, continuous, 200 μA beam of 1 keV electrons about 1 mm in diameter. The electron beam crosses the free jet expansion perpendicular to the direction of flow and at a 45° angle with respect to the axis of the primary TOF mass spectrometer (which is also perpendicular to the free jet expansion). By adjusting the deflectors, the electron beam can be positioned precisely in the free jet expansion. The vertical distance between the aperture of the pulsed valve and the electron beam crossing can be varied from 0.1 to 2.5 cm. The pulsed valve, electron beam source, and a Faraday cup used to monitor the electron beam are mounted on a rigid assembly which can be translated from outside the vacuum system. This allows the distance Z (see Fig. 1) between the electron beam crossing and extraction into the primary TOF mass spectrometer to be varied from 0 to 20 cm, while the electron beam to pulsed valve distance remains constant.

The production of a neutral plasma is the key to the generation of large numbers of positively and negatively charged clusters by the electron beam/pulsed free jet expansion combination. The initial interaction of the 1 keV electrons and the expanding gas results primarily in the production of small positive ions and low energy secondary electrons. This combination of positive ions and low energy electrons produces an electrically neutral plasma with a relatively high ion density and a low loss rate of ions, features crucial to the efficient formation of cluster ions. The neutral plasma confines the high initial ion concentration, approximately 10^9 cm^{-3}, which would otherwise decrease quickly due to Coulomb repulsion in the ionic cloud. The neutral plasma also shields itself from external fields and remains collisionally coupled to the free jet expansion, allowing the use of long drift distances (at least 20 cm) without significant loss of ions.

The large drift distances (and resulting long reaction times) are important to the reactive formation of both positively and negatively charged cluster ions. By slowing the rate of diffusion of the ions, the neutral plasma environment allows the ions to experience many low energy ion–neutral collisions. Three body collisions in the high density region allow small cluster ions to grow via association reactions. Two body collisions allow further growth and stabilize metastable cluster ions. Since the Langevin ion–neutral two body collision rate is temperature independent, it decreases only with the decreasing density of the expanding jet, much more slowly than the neutral–neutral two body collision rate in the low temperature free jet expansion.

In these experiments a mixture of 1% Br_2 in CO_2 at a total pressure of 2 atm was used to generate the mixed ionic clusters. The electron beam crossed the expansion 0.5 cm below the valve aperture and the ion drift distance Z was 15 cm, corresponding to a reaction time >0.3 ms. Under these conditions substantial amounts of $Br_2^- \cdot (CO_2)_n$, $n \leqslant 24$, were produced without excessive interference from other species.

C. Primary TOF mass analysis and photolysis

Following the field free drift region, ions are extracted perpendicular to the expansion axis by applying a 1000 V pulse across a pair of electrodes, as shown in Fig. 1. This extraction pulse forms the first acceleration region of a Wiley–McLaren style TOF mass spectrometer,[34] modified to accommodate the 2–3 cm spatial spread of the ions produced by the electron beam/pulsed free jet expansion ion source. The spatial extent of the ions is considerably larger than that typically obtained by laser ionization and requires different design parameters. The use of a skimmer prior to extraction would give a smaller spatial distribution, but it would also reduce the number of ions injected into the mass spectrometer. A 5 cm spacing between the electrodes in the first acceleration region was chosen to utilize most of the spatial distribution of the ions and to avoid perturbing the flow characteristics of the unskimmed expansion. Design of the primary TOF mass spectrometer was determined chiefly by this choice of spacing.

The extraction pulse, produced by a simple thyratron circuit, has a sharp leading edge (10^{11} V/s) followed by a long decay (100 μs time constant). The decay time is long enough such that the extraction voltage is approximately constant over the time the largest ionic clusters take to exit the extraction region (10 μs), as required to obtain optimal focusing of the spatial distribution. After passing through the entrance aperture (3 mm in diameter), the ions acquire an additional 2.5 keV of kinetic energy over a distance of 5 cm in the second acceleration region of the primary TOF mass spectrometer. A series of guard rings maintains parallel field conditions in this region. Disruption of the hydrodynamic flow of the free jet is mitigated by minimizing the size of the second acceleration region, enclosing it in a small tube 8 cm in diameter and 20 cm long. This tube also serves, in conjunction with the entrance aperture, both as a conductance barrier for the differentially pumped flight tube and a shield for the ions in the free jet expansion from the electric field of the second acceleration region. Following the second acceleration region, the ions pass through a set of vertical deflectors which compensate for most of the small downward component of kinetic energy imparted by the supersonic beam. Ions then pass through an einzel lens tuned to focus the ions transversely at the longitudinal focus of the primary TOF mass spectrometer, 1.5 m from the entrance aperture. The transverse focus is accomplished by running the einzel lens in a mild decelerating mode with the central element set at 1.5 kV. This has no significant effect on the timing of the primary TOF mass spectrometer. Immediately following the einzel lens the ion beam is deflected 1.5° by a set of horizontal deflectors. This small deflection reduces the background signal at the neutral photofragment detector.

The ion beam is crossed perpendicularly by the laser pulses at the spatial focus of the primary TOF mass spectrometer. The ionic clusters arrive at the spatial focus at a

time determined by their mass. Thus, the time delay of the laser pulse relative to the extraction pulse of the primary TOF mass spectrometer unambiguously determines the mass of the ion cluster being probed. The photodissociation studies of $Br_2^- \cdot (CO_2)_n$ were carried out at wavelengths of 355, 700, and 820 nm. The laser fluence typically used was 1–2 mJ/cm^2 at 355 nm and 20–30 mJ/cm^2 at 700 and 820 nm. Laser output was generated by a YAG pumped dye laser system (Quanta Ray DCR-1A and PDL-1). Multiphoton processes are easily detected as laser fluence dependent fragmentation patterns, allowing the extent of multiphoton processes to be determined accurately. Multiphoton processes were not observed for the typical laser fluences used.

D. Secondary TOF mass analysis and detection

Mass analysis of the ionic photofragments is achieved by the secondary TOF mass spectrometer which uses a modified reflectron[35] both to reverse the trajectories of the ions and to separate parent and fragment ions according to their mass. The primary utility of the reflectron for our experiments lies in the fact that a mode of operation exists where the arrival times at the ion detector of fragment ions from given mass parent ions are strongly dependent on the fragment mass but only weakly dependent on the parent ion kinetic energy.

In order to understand this mode of reflectron operation, we first examine how a reflectron refocuses parent ions. The reflectron design used in this instrument consists of a reversing field tilted a small angle off the beam axis followed by a field free drift region, as depicted schematically in Fig. 2(a). Consider two ions of the same mass m located at the entrance and moving into the reflectron, one with energy U_1 and one with energy U_2. This is the situation for ions generated by the electron beam/pulsed free jet expansion ion source and spatially focused near the entrance of the reflectron. The ion with more energy penetrates more deeply into the field of the reflectron and exits later in time. After leaving the reflectron, the more energetic ion eventually catches up to the less energetic ion at the second spatial focus of the tandem TOF mass spectrometer, the location of the ion detector.

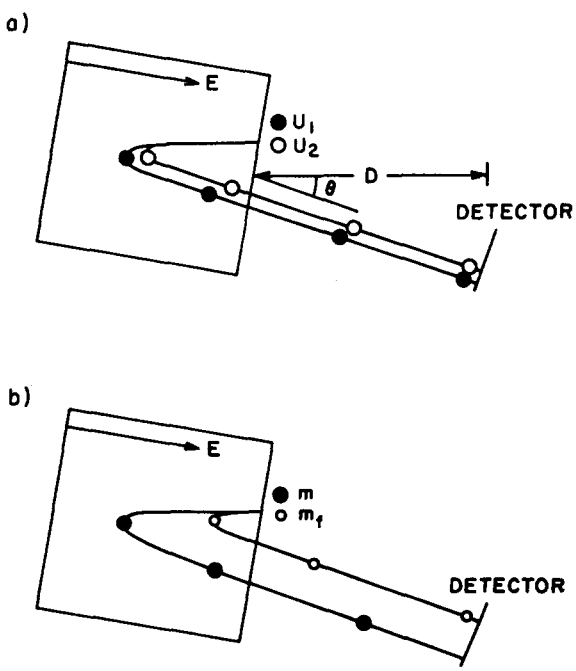

FIG. 2. A schematic diagram of the reflectron depicting (a) the refocusing of two ions of the same mass m but different energies, U_1 and U_2, and (b) the separation of fragment ions of mass m_f from parent ions of mass m. The filled and unfilled dots represent the trajectories of the two groups of ions.

To calculate the distance to the second spatial focus we first calculate the time T required for an ion to travel from the entrance of the reflectron through the reversing field and to the ion detector:

$$T = [2m \sec(\theta/2)/qE\,](2U/m)^{1/2} + D \sec\theta/(2U/m)^{1/2}, \tag{2.1}$$

where E is the magnitude of the reversing electric field, $(2U/m)^{1/2}$ is the initial (and final) velocity of the ion, D is the distance from the reflectron to the ion detector and θ is the tilt angle of the reflectron. The spatial focus occurs where $dT/dU = 0$, namely at

$$D = 4\langle U\rangle/qE, \tag{2.2}$$

where $\langle U\rangle$ is the average kinetic energy of the parent ions.

Next we consider how the reflectron can function as a mass analyzer for ionic photofragments. Figure 2(b) shows a parent ion of mass m, a fragment ion of mass m_f and their trajectories through the reflectron. It can be seen in Fig. 2(b) that the parent ion penetrates further into the reflectron and arrives at the ion detector later in time and at a different transverse location. The distance to the second spatial focus for ionic photofragments can be obtained by rewriting Eq. (2.1) for the time required for fragment ions to travel from the entrance of the reflectron to the ion detector:

$$T = [2m_f \sec(\theta/2)/qE\,](2U/m)^{1/2} + D \sec\theta/(2U/m)^{1/2}. \tag{2.3}$$

Note that the transit time depends linearly on the mass of the fragment ion, for a given mass parent ion. This is because fragment ions from parents of mass m have the same initial (and final) velocity, $(2U/m)^{1/2}$, regardless of their mass, but have different energy. The fragment energy U_f is simply the ratio of the fragment mass to the parent mass times the parent energy, $(m_f/m)U$. For fragment ions the distance to the spatial focus is $4\langle U_f\rangle/qE$. Clearly for fixed reflectron field strength E the distance to the spatial focus depends on the mass of the fragment ion. By reducing the reflectron field strength to the value

$$E_f = (m_f/m)E, \tag{2.4}$$

fragment ions of mass m_f will be spatially focused at the same distance D that the parent ions are by the reflectron field strength E. The focused fragment ions also spend *exactly* the same time in transit to the ion detector as their parents did, providing unambiguous fragment ion mass determination. In addition, since the focused fragment ions follow the same trajectory as their parents, they will strike the detector in the same area, eliminating possible problems of spatially

varying detection efficiency. This arrangement unfortunately precludes detection of all fragment ions from each laser pulse, but affords an unambiguous method of determining the mass of the fragment ion.

The reflectron is 20 cm deep and 15 cm in diameter. Wire mesh at both ends allows particles to enter and exit the retarding field region while maintaining a uniform electric field within the reflectron. The entrance to the reflectron is held at the beam potential, 2.5 kV, and the rear is biased so the ions of interest are reflected at 50%–90% of the total depth, -3.5 kV to -830 V for parent ions. Ten guard rings, 0.4 in. thick, spaced by 0.021 in. thick Mylar washers and connected by resistors drop the potential smoothly between the ends and maintain field homogeneity. The entire assembly is tilted 10°, displacing the reflected ions 20° from the incident beam to allow room for the ion detector.

The ion detector (Johnston MM1) and a series of parallel wire acceleration meshes are mounted in an aluminum cylinder to shield the ion beam from the detector bias potential. A small potential, approximately 200 V, is applied to the first mesh to discriminate against low energy electrons. The second mesh accelerates ions an additional 3 keV just before striking the detector. The additional kinetic energy is particularly important for efficient detection of the very light (low energy) ionic fragments produced by photodissociation of large parent ions. Signal levels are usually in the range of 10^2–10^6 ions per valve opening, which requires the detector to be operated in a linear rather than a particle counting mode.

A particle multiplier (Ceratron series EME) located behind the reflectron along the primary TOF axis allows detection of neutral particles resulting from photodissociation or photodetachment of ions. Neutral photofragments from a given parent ion are obviously not separated in the reflectron and all arrive at the neutral detector simultaneously. The number of neutral fragments typically exceeds 100 from each laser pulse, so this multiplier must also be operated in a linear gain mode.

Under our operating conditions, $\langle U \rangle = 3$ keV, $D = 20$ cm, and $\theta = 20°$, we estimate a mass dispersion of 50 ns/amu for a fragment ion of mass 100 amu from a parent ion of mass 500 amu. The typical width of a mass peak is 70 ns (FWHM), so identical masses are well focused while different masses are dispersed. We normally attain a fragment ion mass resolution > 50, even though the energy resolution $U/\Delta U$ of the parent ion beam is only 5.

E. Data collection

In the negative ion mode of operation, after ion acceleration and electron amplification, the anode potential of the ion detector reaches 10 kV, requiring capacitive coupling of the ion signal to the pulse processing electronics. The signal is preamplified (Ortec 9301) and sent to a transient digitizer/signal averager (Transiac 2001S/4100). Dwell time, record length, and the number of averages are controlled by a computer (DEC MINC-11), which also reads the data from the signal averager and stores it on a disk after completion of the preset number of averages.

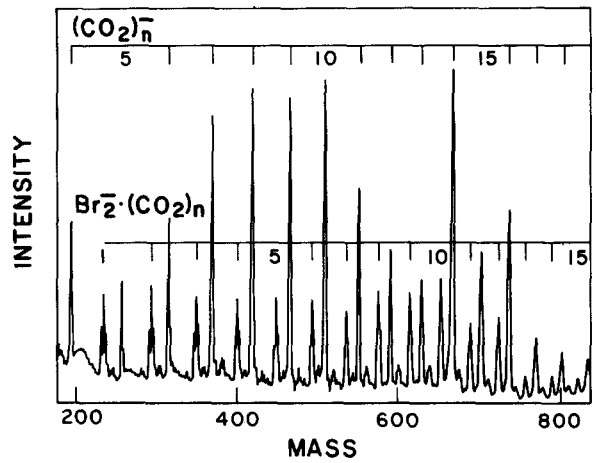

FIG. 3. A typical parent ion mass spectrum. The major species are $(CO_2)_n^-$ and $Br_2^-\cdot(CO_2)_n$ clusters. In addition, $Br^-\cdot(CO_2)_n$ clusters are present in the lower mass region while $Br_4^-\cdot(CO_2)_n$ clusters are present in the higher mass region.

Figure 3 shows a parent ion mass spectrum taken under the typical conditions described previously. This spectrum was taken at 20 ns dwell time and is an average of 128 openings of the pulsed valve. Several classes of cluster ions are present in the mass spectrum, $Br^-\cdot(CO_2)_n$, $Br_2^-\cdot(CO_2)_n$, $Br_4^-\cdot(CO_2)_n$, and $(CO_2)_n^-$ clusters. The parent ion mass resolution, $M/\Delta M$, is about 200, more than enough for separation of these species. Multiplets due to the isotopes of bromine are easily resolved up to mass 500, making the assignment of this portion of the mass spectrum especially easy. Arrival times of higher mass cluster ions are readily calculated by extrapolation from the arrival times of the lower mass cluster ions.

The acquisition of photofragmentation data involves some additional steps. The laser timing is adjusted to allow the laser pulses to strike the selected parent cluster ion and the reflectron voltage is adjusted to focus the fragment ion of interest. The laser timing is set by observing, on an oscilloscope, either the depletion of a given parent ion peak or the production of neutral photofragments. The latter method is much more sensitive and was used for the 700 and 820 nm data. The computer sets the reflectron voltage for the selected fragment ion mass, as discussed above, and directs the signal averager to record data for a number of openings of the pulsed valve with the laser striking the selected cluster ion and the same number with it blocked. This process is repeated for each fragment ion from each parent ion. The photofragmentation data presented here are the result of 800 openings of the pulsed valve (400 with the laser striking the selected ion and 400 with it blocked) per fragment ion.

The branching ratios for photofragmentation of a given parent ion are determined by integrating the stored fragment ion mass peaks and scaling the results to compensate for the momentum dependent detection efficiency of the ion detector. The scaling relationship for detection efficiency was determined by comparing the absolute amount of signal depleted from a parent cluster peak with the amount appearing as fragment ion signal. This quantity was measured for several

different ions and a variety of energies, and found to vary approximately linearly with momentum over the energy range of interest. While this approximate dependence was used to scale the raw data, it does not materially affect the results.

III. RESULTS AND DISCUSSION

The primary goal of this work is to study the photodissociation and recombination dynamics of Br_2^- in $Br_2^- \cdot (CO_2)_n$ clusters. The first section reports the photofragmentation products generated by photoexcitation of the cluster ions. Before drawing conclusions about the dynamics of photodissociation and recombination from the data, three relevant issues will be addressed. First, we present evidence that the identity of the chromophore within the cluster is Br_2^-. Second, the contention that the Br_2^- chromophore dissociates following photoabsorption will be substantiated. Third, data will be presented which argue that recombination has actually occurred in the Br_2^- based photofragments. Finally, the photofragmentation data are interpreted in terms of the dynamics of photodissociation and recombination.

A. Photofragmentation data

Photoabsorption by a given $Br_2^- \cdot (CO_2)_n$ cluster results in the production of two types of ionic photofragments: Br_2^- based fragments

$$Br_2^- \cdot (CO_2)_n + h\nu \rightarrow Br_2^- \cdot (CO_2)_m + (n-m)CO_2, \quad (3.1)$$

and Br^- based fragments

$$Br_2^- (CO_2)_n + h\nu \rightarrow Br^- \cdot (CO_2)_k + Br + (n-k)CO_2. \quad (3.2)$$

Identification of the ionic products is straightforward, even when both types of products are present. For example, Fig. 4 shows Br_2^- and $Br^- \cdot (CO_2)_2$ fragments resulting from absorption of a 700 nm photon by $Br_2^- \cdot (CO_2)_5$. The Br_2^- fragment is easily distinguished from the Br^- based fragment by the triplet vs doublet isotope splitting as well as by the arrival time.

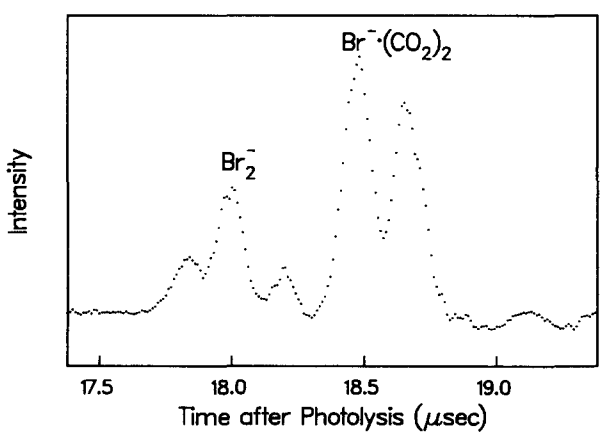

FIG. 4. Two ionic photofragments, Br_2^- (158, 160, and 162 amu for $^{79}Br_2^-$, $^{79}Br^{81}Br^-$, and $^{81}Br_2^-$, respectively) and $Br^- \cdot (CO_2)_2$ (167 and 169 amu for the $^{79}Br^-$ and $^{81}Br^-$ isotopes, respectively), arising from the photofragmentation of $Br_2^- \cdot (CO_2)_5$ at 700 nm.

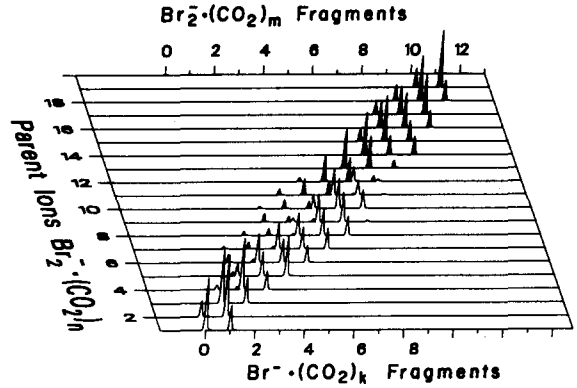

FIG. 5. A schematic representation of the ionic photofragments from $Br_2^- \cdot (CO_2)_n$, $n = 1$–19, at 700 nm. The peaks lying along a given horizontal line represent the ionic photofragments from a given parent ion. Br^- based photofragments are unshaded and are labeled by the axis at the bottom. Br_2^- based photofragments are shaded and labeled by the axis at the top.

A representation of the 700 nm photofragmentation data for $Br_2^- \cdot (CO_2)_n$, $n = 1$–19, is shown in Fig. 5. The uncertainty is approximately 5% of the height of the peak. The 700 nm photofragmentation data show only Br^- based fragment ions for $n < 4$. Both types of fragment ions are observed for n = 4–12. For $n \geqslant 13$, only Br_2^- fragments are observed. The photofragmentation data at 820 nm are similar, except that Br_2^- based fragment ions are first observed at $n = 2$. For 355 nm excitation, Br_2^- based fragments are not observed until $n = 11$.

The branching ratio for production of Br_2^- based fragment ions (the number of Br_2^- based fragments divided by the total number of ionic photofragments) vs cluster size for the wavelengths studied is plotted in Fig. 6. For 700 and 820 nm excitation, the data can be divided into three regions:

(I) A small cluster region, $n \leqslant 10$, where most of the ionic fragments are Br^- based.

(II) An intermediate transition region from $n = 10$–13.

(III) A large cluster region, $n \geqslant 13$, where the only ionic fragments observed are Br_2^- based.

The branching ratio in region I is strongly dependent on photon energy, decreasing by as much as a factor of 2

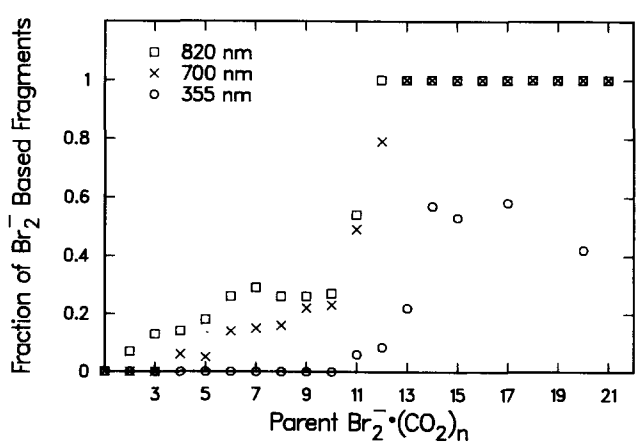

FIG. 6. The branching ratio for production of Br_2^- based ionic photofragments vs parent cluster ion size for 355, 700, and 820 nm excitation.

between 820 and 700 nm excitation. Region II is dominated by a sharp rise in branching ratio, reaching 100% at $n = 13$. In the third region, only Br_2^- based ionic fragments are observed, independent of both cluster size and photon energy. Additional ionic photofragments corresponding to absorption of two photons are observed at higher laser fluences for $n > 4$ at 700 nm and $n > 2$ at 820 nm. These photofragments are less massive than the one photon fragments, and have intensities proportional to the square of the laser fluence.

The 355 nm data in Fig. 6 also display three regions. In the small cluster region the 355 nm data show no detectable Br_2^- based fragments. A rapid increase in branching ratio occurs from $n = 12$–14. For larger clusters the branching ratio is approximately constant at 50%.

B. Photoabsorption and electronic structure of $Br_2^-\cdot(CO_2)_n$

We contend that the charge in the $Br_2^- \cdot (CO_2)_n$ clusters remains localized on an intact Br_2^-, and furthermore that Br_2^- is the visible chromophore in the cluster ions. This contention seems likely *a priori*, based on studies of the dihalogen negative ions in solution,[36] where features in the vibrational Raman spectra occur at values calculated[37] for isolated Br_2^-. Similarly, studies of alkali metal cations complexed to Br_2^- in an argon matrix[38] indicate that Br_2^- remains the chromophore in the matrix. The remainder of this section discusses evidence relevant to the claim that the charge remains localized on an intact Br_2^- and that Br_2^- is the chromophore in $Br_2^- \cdot (CO_2)_n$ clusters.

A discussion of the energetics of Br_2^- is useful prior to consideration of the electronic structure of $Br_2^- \cdot (CO_2)_n$. The potential energy curves of Br_2^- relevant to the photoabsorption process are shown schematically in Fig. 7. Photoabsorption at 355 nm corresponds to a transition from the $^2\Sigma_u^+$ ground state to the purely repulsive $^2\Sigma_g^+$ excited state. Photoabsorption at 700 or 820 nm results in a transition to the

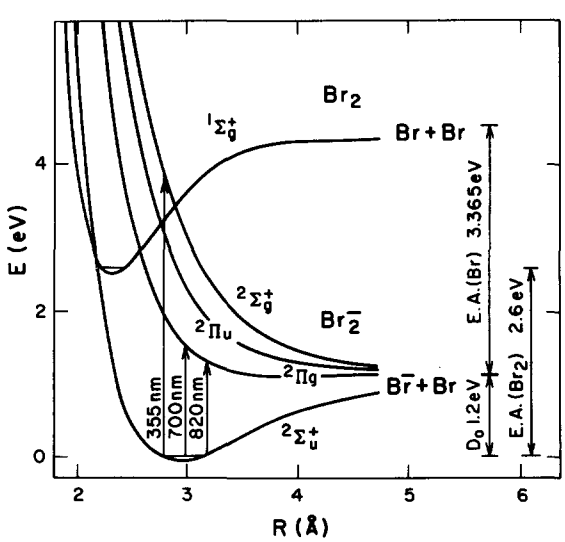

FIG. 7. The relevant potential energy curves for Br_2^- and Br_2. The vertical arrows labeled by wavelength are intended to show schematically which excited state is accessed at a given wavelength.

$^2\Pi_g$ state, which is also repulsive. It is clear that photoabsorption leads to photodissociation with unit quantum efficiency. Although no photodissociation data are available for gas phase Br_2^-, there have been photodissociation studies of Cl_2^-,[39,40] which suggest that the $^2\Pi_u$ state may be weakly bound.[40] The potential energy curves in Fig. 7 were taken from the calculations of Wadt and Hay.[41] The asymptotic energies have been adjusted to agree with experimental values for the electron affinity (EA) of Br_2 and the dissociation energy (D_0) of Br_2^-. The EA of Br_2 has been determined to be 2.6 ± 0.2 eV by endoergic charge transfer.[42] There are no direct measurements of $D_0(Br_2^-)$ in the gas phase; however a reasonable estimate can be obtained from a thermodynamic cycle that uses the EA of Br_2, $D_0(Br_2)$, 1.971 eV,[43] and the EA of Br, 3.365 eV[44]:

$$D_0(Br_2^-) = D_0(Br_2) + EA(Br_2) - EA(Br) .$$

This yields a Br_2^- bond energy of 1.2 ± 0.2 eV. Raman studies of Br_2^- in solution yield a similar value, 1.3 ± 0.2 eV, via Birge–Sponer extrapolation.[36] Based on this bond energy, photoabsorption of 820 nm (1.5 eV), 700 nm (1.8 eV), or 355 nm (3.5 eV) photons by Br_2^- gives, respectively, 0.3, 0.6, or 2.3 eV kinetic energy to the nascent atoms.

In the $Br_2^- \cdot (CO_2)_n$ clusters, the Br_2^- species is expected to be stable based on energetic grounds. Especially clear is the case of the binary complex $Br_2^- \cdot (CO_2)$, where consideration of only a few alternative charge distributions is required: $Br_2 \cdot CO_2^-$, $[Br_2CO_2]^-$, and $Br \cdot CO_2 \cdot Br^-$. The $Br_2 \cdot CO_2^-$ form is very unlikely since CO_2^- is unstable by 0.6 eV[45] with respect to $CO_2 + e^-$. This implies that this configuration is less stable than $Br_2^- \cdot CO_2$ by 3.2 eV (the EA of Br_2 plus an additional 0.6 eV required to force the electron onto a CO_2 monomer). Since the addition of an electron to CO_2 is endoergic, even a partial charge transfer described by $(Br_2 \cdot CO_2)^-$ would appear to be unfavorable. The $Br \cdot CO_2 \cdot Br^-$ structure is also unlikely, since it costs the bond energy of Br_2^- (1.2 eV) and recovers only the difference between the EAs of Br_2 and Br (0.75 eV) and the differential solvation energy between the $Br \cdot CO_2 \cdot Br^-$ and the $Br_2^- \cdot CO_2$ structures.

For larger clusters, the possibility of $Br_2 \cdot (CO_2)_n^-$ competing with $Br_2^- \cdot (CO_2)_n$ can similarly be ruled out energetically. DeLuca *et al.*[46] have measured photoelectron spectra of $(CO_2)_n^-$ clusters, $n = 2$–13, and observe that the EA of the corresponding neutral cluster is less than ≈ 2.2 eV. Since the EA of Br_2 is 2.6 eV, the charge transfer reaction $Br_2^- + (CO_2)_n \rightarrow Br_2 + (CO_2)_n^-$ is endothermic at least for $n < 14$. The positive electron affinity of the larger $(CO_2)_n$ clusters does not, however, preclude the possibility of some charge sharing in the larger clusters. Regarding the $Br \cdot (CO_2)_n \cdot Br^-$ class of structures, where the bromine atoms are separated, it seems likely, in analogy with the binary $Br_2^- \cdot CO_2$ complex, that the energy gained is less than $D_0(Br_2^-)$. These structures are therefore unlikely to be more stable than $Br_2^- \cdot (CO_2)_n$. Based on these energetic arguments, we contend that the $Br_2^- \cdot (CO_2)_n$ configuration is the most stable. Detailed electronic structure calculations on these species are not available, but would be most welcome.

Since the clusters are formed by association of CO_2 monomers onto the Br_2^- core, the existence of a kinetic bottleneck inhibiting the formation of the most stable structure is unlikely.

We have no direct spectroscopic evidence that $Br_2^- \cdot (CO_2)_n$ correctly describes the clusters in this experiment, however, the photodissociation data support the contention. We observe that free Br_2^- has a small photodissociation cross section at both 820 and 700 nm, exhibits no photodissociation at 532 nm, and has a large photodissociation cross section at 355 nm, approximately 20 times larger than the photodissociation cross section at 700 and 820 nm. All of the $Br_2^- \cdot (CO_2)_n$ clusters studied here display very similar photodissociation behavior. In contrast, neither $Br^- \cdot (CO_2)_n$ or $(CO_2)_n^-$ clusters show detectable photodissociation at 700 or 820 nm. These observations are a strong indication that Br_2^- is the chromophore for all of the clusters studied here.

Supporting evidence for a Br_2^- chromophore also comes from the photofragmentation data. Photolysis of $Br_2^- \cdot (CO_2)_n$ at 355 nm always yields some Br^- based photofragments. The existence of these products following 355 nm excitation suggests that the photon energy is localized in the Br–Br^- bond and that the $^2\Sigma_g^+ \leftarrow {}^2\Sigma_u^+$ transition of Br_2^- is intact for all clusters studied. Thus, it seems reasonable to assume that photoabsorption at 700 and 820 nm is due to the $^2\Pi_g \leftarrow {}^2\Sigma_u^+$ transition of Br_2^- for all of the clusters studied. These results support the contention that the electron remains localized on Br_2 in the clusters studied and that the electronic structure of clustered Br_2^- is qualitatively unchanged from that of free Br_2^-.

The photofragmentation behavior of other cluster ions also supports the existence of a Br_2^- chromophore in $Br_2^- \cdot (CO_2)_n$ clusters. Photolysis of $(CO_2)_n^-$ clusters at 355 nm results[33] in evaporation of neutral CO_2 molecules for $n \geqslant 13$, and thus only Br_2^- based and $(CO_2)_n^-$ ionic photofragments would be expected from photofragmentation of large $Br_2^- \cdot (CO_2)_n$ clusters if the charge had completely left Br_2. Since only Br^- and Br_2^- based photofragments are observed from $Br_2^- \cdot (CO_2)_n$, the electron appears to be at least partially localized on Br_2. Photodetachment is the only channel observed following absorption of 355 nm photons by $Br^- \cdot (CO_2)_n$ clusters, i.e., no ionic photofragments are observed. This is not the behavior observed for the $Br_2^- \cdot (CO_2)_n$ clusters and implies that Br_2^- is intact within the $Br_2^- \cdot (CO_2)_n$ clusters.

Based on the combined strength of these arguments, we conclude that the charge remains localized on Br_2, and that Br_2^- is the absorber for all the clusters investigated in the present work. This is equivalent to concluding that the gross electronic structure of the parent cluster ions is of the form $Br_2^- \cdot (CO_2)_n$ and *not* $Br_2 \cdot (CO_2)_n^-$, $[Br_2 \cdot (CO_2)_n]^-$, or $Br \cdot (CO_2)_n \cdot Br^-$.

C. Photodissociation of Br_2^-

Both the photofragmentation and the photodissociation data indicate that the Br_2^- chromophore dissociates following photoabsorption. The observation of Br^- based photofragments clearly indicates dissociation of Br_2^- in some of the absorbing clusters. The most direct evidence that Br_2^- is initially dissociated in *all* of the absorbing clusters is the similarity of the cluster ion photodissociation cross section to that of free Br_2^-.

With 355 nm excitation, some Br^- based photofragments are always observed, indicating that excitation occurs, at least partially, to a dissociative state. With 820 and 700 nm excitation, only Br_2^- based fragments are observed for the larger clusters, and, as a result the case is less clear. Because the excess energy at 820 and 700 nm (0.3 and 0.6 eV, respectively, above the dissociation energy of free Br_2^-) is close to the energy of solvation, it is possible that the disappearance of Br^- based photofragments at $n = 13$ results from a solvation effect producing a bound upper state. If this were the case it is likely that the photodissociation cross section would change, including, perhaps, the appearance of structure in the cross section as a function of wavelength. The similarity in photodissociation cross section for all of the cluster ions studied and the lack of any structure observed as a function of wavelength near 700 and 820 nm in any of the ionic clusters, argues that photoabsorption always results in dissociation of Br_2^- in the $Br_2^- \cdot (CO_2)_n$ cluster ions.

D. Recombination of the dissociated Br_2^-

Examination of the fragmentation data indicates that Br_2^- has recombined within the fragment ion clusters which contain two Br atoms, i.e., the structure of the Br_2^- based fragment ions is $Br_2^- \cdot (CO_2)_m$, not $Br^- \cdot (CO_2)_m \cdot Br$. At increased laser fluence the 700 nm fragmentation products of $Br_2^- \cdot (CO_2)_n$, with $n > 4$, include small amounts of small Br^- based photofragments. The quantity of these Br^- based photofragments depends on the square of the laser fluence, indicative of a two photon process. Since $Br^- \cdot (CO_2)_n$ and presumably $Br \cdot (CO_2)_n$ do not absorb 700 nm radiation, these fragments probably result from absorption of a second photon by the *recombined* Br_2^-, i.e.,

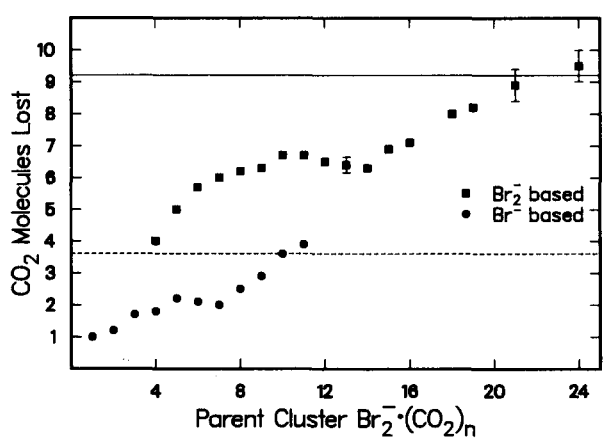

FIG. 8. The average number of CO_2 molecules lost after absorption of a 1.8 eV photon for both Br_2^- and Br^- based photofragments as a function of parent cluster ion size. The solid horizontal line shows the predicted maximum average number of CO_2 molecules lost for 1.8 eV excitation. The dashed horizontal line shows the predicted maximum average number of CO_2 molecules lost for 0.6 eV excitation.

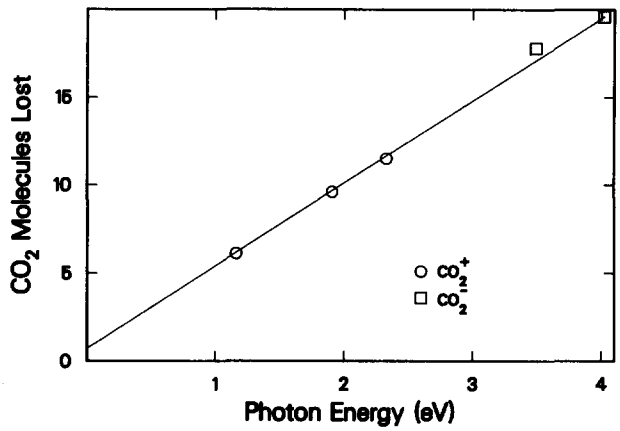

FIG. 9. The maximum average number of CO_2 molecules lost from $(CO_2)_n^+$ and $(CO_2)_n^-$ as a function of photon energy. The horizontal lines in Fig. 8 represent data taken from this graph.

$$Br_2^- \cdot (CO_2)_n \xrightarrow{h\nu} Br_2^- \cdot (CO_2)_m \xrightarrow{h\nu} Br^- \cdot (CO_2)_j, \quad n > m > j .$$

Additional evidence that the dissociated Br_2^- has recombined in the Br_2^- based photofragments comes from analysis of the number of CO_2 molecules lost following photoabsorption. The average number of CO_2 molecules lost following photoabsorption at 700 nm (1.8 eV) as a function of parent cluster ion size for both Br^- and Br_2^- based photofragments is shown in Fig. 8. The average number of CO_2 molecules remaining on Br_2^- based photofragments is *always* less than the average number remaining on Br^- based photofragments from the same parent ion.

The horizontal lines in Fig. 8 are derived from the data in Fig. 9, a plot of the average number of CO_2 molecules lost in the photofragmentation of large $(CO_2)_n^+$ $(n > 20)$ and $(CO_2)_n^-$ $(n > 35)$ clusters[32,33] as a function of excitation energy. For the large clusters the average number of CO_2 molecules lost is linearly dependent on the excitation energy but independent of the parent cluster ion size or the sign of the charge. The average number of CO_2 molecules lost from smaller clusters is less than the average lost from larger clusters, for a given excitation energy, and decreases with decreasing cluster size. Thus, the average energy expended per CO_2 molecule lost in the smaller clusters is more than that expended in the larger clusters. Figure 9, therefore, represents the *maximum* average number of CO_2 molecules lost, as a function of excitation energy, in the photofragmentation of $(CO_2)_n^-$ or $(CO_2)_n^+$ cluster ions. Similarly, the slope of the data in Fig. 9 represents the *minimum* average energy required to remove one CO_2 molecule from a $(CO_2)_n^-$ or $(CO_2)_n^+$ cluster ion.[32,33] The solid line in Fig. 8 corresponds to the loss of 9.2 CO_2 molecules, the maximum expected average loss with 1.8 eV of excess energy. The dashed line in Fig. 8 corresponds to the loss of 3.6 CO_2 molecules, the maximum expected average loss with 0.6 eV [1.8 eV—$D_0(Br_2^-)$] of excess energy.

For the Br_2^- based photofragments, the average number of CO_2 molecules lost is consistent with all of the excitation energy becoming available for evaporation of CO_2 molecules. Conversely, the number of CO_2 molecules lost is inconsistent with only 0.6 eV available for evaporation of CO_2 molecules. This observation implies that a preponderance of the energy initially expended to break the Br_2^- bond is recovered by recombination. For the Br^- based photofragments, the number of CO_2 molecules lost is consistent with that expected if only 0.6 eV is available for evaporation of CO_2 molecules.

E. Dynamics of photodissociation and recombination

Having concluded that Br_2^- is the chromophore for all the clusters studied here, and that following photodissociation, recombination of Br_2^- occurs in the Br_2^- based photofragments, the dynamics of photodissociation and the subsequent recombination can now be addressed. We have measured the dependence of the branching ratio for recombination on two factors: photon energy and parent cluster ion size. The results are summarized below.

For the photon energies studied, the branching ratio for recombination vs parent cluster ion size (Fig. 6) can be divided into three regions:

(I) In the region from $n = 2$–10, the branching ratio for recombination is small, increases gradually with parent cluster ion size and is strongly dependent on the photon energy.

(II) For parent cluster ion sizes of $n = 10$–14, the branching ratio for recombination displays a strong dependence on parent cluster ion size regardless of the photon energy.

(III) For parent cluster ion sizes of $n \geqslant 14$, only recombined ionic photofragments are observed for 700 and 820 nm excitation. For 355 nm excitation the branching ratio is approximately 50%. A weak dependence on photon energy and no dependence on parent cluster size are observed in this cluster size regime.

The caging mechanism operative for small clusters appears to be controlled primarily by the photon energy, probably by the kinetic energy of the nascent Br atoms. A different mechanism is indicated for the large clusters: one largely insensitive to photon energy and parent cluster ion size.

A hard sphere model for the interaction of the nascent Br atoms with the CO_2 molecules does not explain our observations. Calculations on the $(CO_2)_{13}$ neutral cluster by van de Waal[47] indicate that the most stable structure is an isosahedral shell of 12 CO_2 molecules completely surrounding a central CO_2 molecule. If the large $Br_2^- \cdot (CO_2)_n$ clusters had a complete shell of CO_2 molecules, the repulsive interactions of the nascent Br atoms with the CO_2 molecules in the path of the dissociating diatom could lead to recombination following absorption of a sufficiently low energy photon if the collision occurred when Br_2^- was still in the attractive region of its potential. This is essentially the mechanism proposed by Amar and Berne[21] for recombination in large $Br_2 \cdot Ar_n$ clusters. For the smaller ionic clusters a distribution of structures, principally without nearly collinear CO_2 molecules, could explain the observed low occurence of recombination. However, the difference in the photon energy dependence of the branching ratio between small and large ionic clusters is difficult to explain with this purely repulsive model; a more

sophisticated model incorporating the effects of intermolecular attraction is indicated.

The photodissociation of Br_2^- in $Br_2^- \cdot Ar_n$ clusters has been studied recently by Amar.[22] The equilibrium structures calculated for the $Br_2^- \cdot Ar_n$ clusters show that for $n < 10$ all of the Ar atoms lie about the interatomic axis of Br_2^-. The only way Ar atoms in this configuration can cage a dissociating Br_2^- is by collectively attracting the nascent atoms, since no small impact parameter collisions between the Br and Ar atoms occur. Amar's molecular dynamics calculations show that this is the case for $Br_2^- \cdot Ar_8$. Since the branching ratio for recombination is determined by a balance between the kinetic energy of the nascent Br and Br^- and their attraction to the surrounding Ar atoms, the branching ratio should depend strongly on excitation energy. The branching ratio for recombination of small $Br_2^- \cdot (CO_2)_n$ clusters depends sensitively on photon energy. Although the structure of $Br_2^- \cdot (CO_2)_n$ is not known, we suggest that an attractive mechanism may also apply to small $Br_2^- \cdot (CO_2)_n$ clusters. For kinetic energies much larger than the attractive interaction, e.g., following 355 nm excitation, no recombination occurs.

For $Br_2^- \cdot Ar_{10}$, Amar finds that one Ar atom resides in a position nearly collinear with Br_2^-, in the path of the dissociating diatom, and that recombination is principally due to impulsive collisions between the collinear atom and a nascent Br atom. This model suggests that once the repulsive interactions become important, recombination will occur with high probability for low excitation energy and exhibit a weak dependence on cluster size. This impulsive model is probably the mechanism for recombination in $Br_2^- \cdot (CO_2)_n$ with $n > 12$, where 100% recombination is observed for both 1.5 and 1.8 eV excitation. For greater excitation energy, e.g., 3.5 eV, such a model suggests that recombination will occur with lower probability but continue to exhibit a relatively weak dependence on cluster size, as is observed. The mass of the solvent molecules may have a significant effect on the recombination process in this regime, an effect which we have not explored but which is amenable to further experiments.

The transition region observed is due to the transition from attractive to repulsive control of the recombination process. The increase in branching ratio for recombination which begins at $Br_2^- \cdot (CO_2)_{11}$ is possibly due to the appearance of a CO_2 molecule in the path of the dissociating diatom for some of the clusters as a result of a distribution of structures or the effects of large amplitude motion in the cluster. Recombination would be highly likely in these clusters and would lead to an abrupt increase in the measured branching ratio for recombination. Molecular dynamics simulations incorporating thermal averaging would contribute to understanding this transition.

V. SUMMARY

We have demonstrated the use of an ion source to synthesize clusters of the form $Br_2^- \cdot (CO_2)_n$. These ion clusters are mass analyzed, photodissociated and the resulting ionic photofragments mass analyzed. Data are presented which imply that the chromophore is Br_2^- for the clusters studied, and that visible and near UV photoabsorption results in dissociation of Br_2^-, followed by recombination in some cases. Two CO_2 molecules are sufficient to cage Br_2^- at a photon energy of 1.5 eV, 0.3 eV above the dissociation limit of free Br_2^-. The minimum number of CO_2 molecules required to cage Br_2^- depends strongly on the photon energy. The branching ratio for recombination vs parent cluster ion size reveals three regions. For small clusters, $n < 10$, the branching ratio for recombination is small for all photon energies used. For clusters with $n = 10$–13, an abrupt transition from a small to a large branching ratio is observed. This transition persists over a wide, 2.0 eV, range of excitation energies. For large clusters, $n > 13$, the branching ratio is large, with *only* recombined ionic photofragments observed following low energy excitation. The data suggest that two mechanisms are responsible for recombination. For small ionic clusters, recombination appears to be due to attractive forces between the CO_2 molecules and the dissociating diatom, while, for large ionic clusters, impulsive collisions of the nascent Br atoms with the CO_2 molecules are largely responsible for recombination.

This ionic system presents an excellent opportunity for a detailed study of the dynamics of photodissociation, recombination, and relaxation. Due to the paucity of low lying electronic states of Br_2^-, all of them repulsive, the complexity concerning nonadiabatic effects in the recombination process is reduced. Furthermore, since photoabsorption is detected extremely sensitively via fragmentation, similar techniques as those described here can be used for picosecond pump–probe measurements.

ACKNOWLEDGMENTS

We are pleased to acknowledge many stimulating discussions with Professor F. Amar. This research was supported by NSF Grant Nos. CHE 83-16628 and PHY 86-04508.

[1] A. W. Castleman and R. G. Keesee, Chem. Rev. **86**, 589 (1986).
[2] J. F. Garvey and R. B. Bernstein, Chem. Phys. Lett. **126**, 394 (1986).
[3] G. Radhakrishnan, S. Buelow, and C. Wittig, J. Chem. Phys. **84**, 727 (1986).
[4] L. Meadows and R. M. Noyes, J. Am. Chem. Soc. **82**, 1872 (1960).
[5] D. Booth and R. M. Noyes, J. Am. Chem. Soc. **82**, 1868 (1960).
[6] E. Rabinowitch and W. C. Wood, Trans. Faraday Soc. **32**, 547 (1936).
[7] H. Hippler, K. Luther, and J. Troe, Chem. Phys. Lett. **16**, 174 (1972).
[8] H. Hippler, K. Luther, and J. Troe, Ber. Bunsenges. Phys. Chem. **77**, 1104 (1973).
[9] K. Luther and J. Troe, Chem. Phys. Lett. **24**, 85 (1974).
[10] J. M. Zellweger and H. Van den Bergh, J. Chem. Phys. **72**, 5405 (1980).
[11] J. C. Dutoit, J. M. Zellweger, and H. Van den Bergh, J. Chem. Phys. **78**, 1825 (1983).
[12] H. Hippler, V. Schubert, and J. Troe, J. Chem. Phys. **81**, 3931 (1984).
[13] K. Luther, J. Schroeder, J. Troe, and U. Unterberg, J. Phys. Chem. **84**, 3072 (1980).
[14] B. Otto, J. Schroeder, and J. Troe, J. Chem. Phys. **81**, 202 (1984).
[15] C. Dupuy and H. Van den Bergh, Chem. Phys. Lett. **57**, 348 (1978).
[16] See G. R. Fleming, *Chemical Applications of Ultrafast Spectroscopy* (Ox-

ford University, New York, 1986), pp. 195–199, and references therein.
[17]V. E. Bondybey, S. S. Bearder, and C. Fletcher, J. Chem. Phys. **64**, 5243 (1976), and references therein.
[18]P. B. Beeken, E. A. Hanson, and G. W. Flynn, J. Chem. Phys. **78**, 5892 (1983), and references therein.
[19]K. L. Saenger, G. M. McClelland, and D. R. Herschbach, J. Phys. Chem. **85**, 3333 (1981).
[20]J. J. Valentini and J. B. Cross, J. Chem. Phys. **77**, 572 (1982).
[21]F. G. Amar and B. J. Berne, J. Phys. Chem. **88**, 6720 (1984).
[22]F. G. Amar, in *The Chemistry and Physics of Small Clusters*, NATO ASI Series, edited by P. Jena, S. Khanna, and B. Rao (Plenum, New York, 1987), p. 207.
[23]H-S. Kim, C-H. Kuo, and M. T. Bowers, J. Chem. Phys. **87**, 2667 (1987), and references therein.
[24]M. E. Geusic, M. F. Jarrold, T. J. McIlrath, R. R. Freeman, and W. L. Brown, J. Chem. Phys. **86**, 3862 (1987), and references therein.
[25]P. Fayet and L. Wöste, Surf. Sci. **156**, 134 (1985).
[26]D. E. Hunton, M. Hofmann, T. G. Lindeman, C. R. Albertoni, and A. W. Castleman, Jr., J. Chem. Phys. **82**, 2884 (1985).
[27]P. J. Brucat, L-S. Zheng, C. L. Petiette, S. Yang, and R. E. Smalley, J. Chem. Phys. **84**, 3078 (1986).
[28]D. E. David, T. S. Magnera, R. Tian, D. Stulik, and J. Michl, Nucl. Instrum. Methods Phys. Res. B **14**, 378 (1986).
[29]C. Bréchignac, Ph. Cahuzac, and J-Ph. Roux, J. Chem. Phys. **88**, 3022 (1988).
[30]A. Stamatovic, F. Howorka, and T. D. Märk, Proceedings of the 6th symposium on Atomic and Surface Physics (SASP), La Plagne, Jan. 1988.
[31]M. A. Johnson, M. L. Alexander, and W. C. Lineberger, Chem. Phys. Lett. **112**, 285 (1984).
[32]M. L. Alexander, M. A. Johnson, and W. C. Lineberger, J. Chem. Phys. **82**, 5288 (1985).
[33]M. L. Alexander, M. A. Johnson, N. E. Levinger, and W. C. Lineberger, Phys. Rev. Lett. **57**, 976 (1986).
[34]W. C. Wiley and I. H. McLaren, Rev. Sci. Instrum. **26**, 1150 (1955).
[35]B. A. Mamyrin, V. I. Karataev, D. V. Schmikk, and V. A. Zagulin, Soviet Phys. JETP **37**, 45 (1973).
[36]G. N. R. Tripathi, R. H. Schuler, and R. W. Fessenden, Chem. Phys. Lett. **113**, 563 (1985).
[37]P. W. Tasker, G. G. Balint-Kurti, and R. N. Dixon, Mol. Phys. **32**, 1651 (1976).
[38]C. A. Wight, B. S. Ault, and L. Andrews, Inorg. Chem. **15**, 2147 (1976).
[39]S. A. Sullivan, B. S. Freiser, and J. L. Beauchamp, Chem. Phys. Lett. **48**, 294 (1977).
[40]L. C. Lee, G. P. Smith, J. T. Moseley, P. C. Cosby, and J. A. Guest, J. Chem. Phys. **70**, 3237 (1979).
[41]W. R. Wadt and P. J. Hay, J. Chem. Phys. **82**, 284 (1985).
[42]P. S. Drzaic, J. Marks, and J. I. Brauman, in *Gas Phase Ion Chemistry*, edited by M. T. Bowers (Academic, New York, 1984), Vol. 3, p. 200.
[43]K. P. Huber and G. Herzberg, *Molecular Spectra and Molecular Structure IV. Constants of Diatomic Molecules* (Van Nostrand Reinhold, New York, 1979), p. 104.
[44]H. Hotop and W. C. Lineberger, J. Phys. Chem. Ref. Data **14**, 731 (1985).
[45]R. N. Compton, P. W. Reinhardt, and C. D. Cooper, J. Chem. Phys. **63**, 3821 (1975).
[46]M. J. DeLuca, B. Niu, and M. A. Johnson, J. Chem. Phys. (submitted).
[47]B. W. van de Waal, J. Chem. Phys. **79**, 3948 (1983).